Theta–gamma coupling increases during the learning of item–context associations

Adriano B. L. Tort[a,b,c,d,1,2], Robert W. Komorowski[e,1], Joseph R. Manns[f], Nancy J. Kopell[c,d,2], and Howard Eichenbaum[e,2]

[a]Edmond and Lilly Safra International Institute of Neuroscience of Natal, Federal University of Rio Grande do Norte, RN 59066, Natal, Brazil; [b]Department of Biochemistry, Federal University of Rio Grande do Sul, RS 90035, Porto Alegre, Brazil; [c]Center for BioDynamics, [d]Department of Mathematics, and [e]Center for Memory and Brain, Boston University, Boston, MA 20215; and [f]Department of Psychology, Emory University, Atlanta, GA 30322
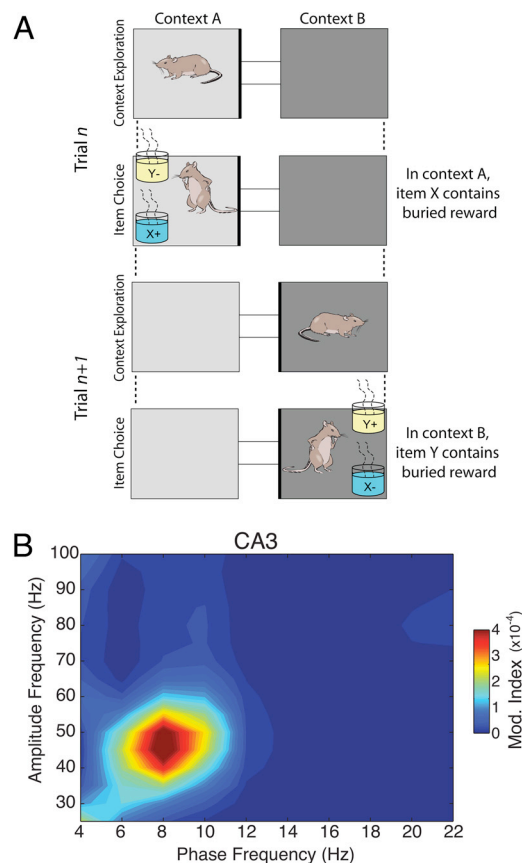
Phase-amplitude cross-frequency coupling (CFC) between theta (4–12 Hz) and gamma (30–100 Hz) oscillations occurs frequently in the hippocampus. However, it still remains unclear whether theta–gamma coupling has any functional significance. To address this issue, we studied CFC in local field potential oscillations recorded from the CA3 region of the dorsal hippocampus of rats as they learned to associate items with their spatial context. During the course of learning, the amplitude of the low gamma subband (30–60 Hz) became more strongly modulated by theta phase in CA3, and higher levels of theta–gamma modulation were maintained throughout overtraining sessions. Furthermore, the strength of theta–gamma coupling was directly correlated with the increase in performance accuracy during learning sessions. These findings suggest a role for hippocampal theta–gamma coupling in memory recall.

associative memory | brain rhythms | local field potential

Fig. 1. Theta phase modulates the LG amplitude in the CA3 region. (*A*) Task scheme. Animals have to learn to associate contexts (represented by different shading) to items (represented by yellow and blue) for reward. A 40-s period of context exploration is allowed before items presentation. The two contexts (A or B) differed in their flooring and walls; the items (X or Y) differed in odor and in the medium that filled the pots. (*B*) Representative phase-amplitude comodulogram computed for a CA3 LFP recorded at *stratum pyramidale* during context exploration.

Brain oscillations have been classically divided into specific frequency ranges associated with multiple cognitive processes (1, 2). Oscillations in these frequency bands may occur simultaneously and can interact with each other (3, 4), suggesting that this coupling may reflect a higher-order representation (5, 6). In one type of interaction, the phase of low-frequency rhythms modulates the amplitude of higher-frequency oscillations (3). This type of cross-frequency coupling (CFC) is called phase-amplitude modulation, and its best known example occurs in the rodent hippocampus between the theta (4–12 Hz) phase and the amplitude of gamma (30–100 Hz) oscillations (6–9). Based on this finding, theoretical work has suggested that gamma and theta oscillations coordinate in support of a neural code (10–15). According to this view, events are represented by distinct neuronal ensembles, each contained within a distinct gamma cycle, and entire episodes are encoded by a succession of event-specific gamma cycles embedded into each theta cycle (12–15). These theories are elegant and appealing, but there is a paucity of evidence linking the existence of theta–gamma coupling to behavior (but see ref. 16). Therefore, it remains unclear whether the hippocampal theta–gamma coupling possesses any functional role (13).

Here, we investigated coupling between theta and gamma rhythms as rats learned which of two stimuli was rewarded depending on the environmental context in which the stimuli were presented. Learning in this type of conditional discrimination task depends on hippocampal function (17, 18). On each trial, a rat initially explored one of two environmental contexts, then the two stimuli were placed into different corners of the environment and the rat was required to choose the correct stimulus for that context to receive a reward (Fig. 1*A*). In our preliminary studies, we found that the initial context exploration period is essential for learning the context-dependent choice. Therefore, we focused on the prominent theta and gamma activity that is prevalent during this period. We found that the strength of theta–gamma coupling in CA3 increases as animals learn and strongly correlates with the increased performance accuracy associated with learning. These findings provide evidence that increases in theta–gamma coupling parallel

learning and signal accurate memory performance. These observations support theoretical models that suggest a functional role for the theta–gamma interaction in information coding.
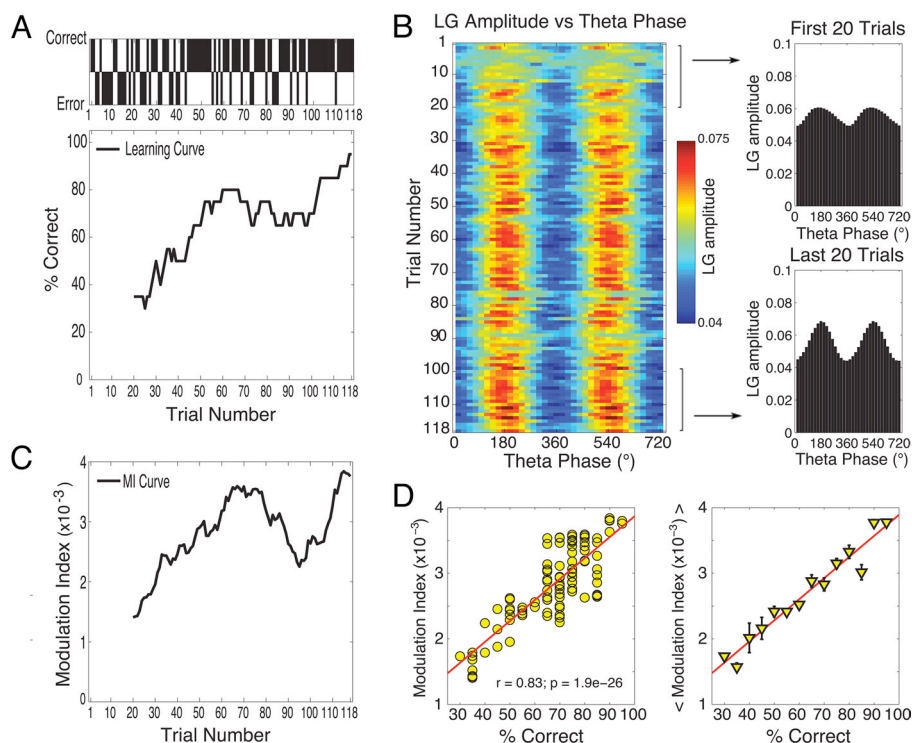

Fig. 2. Theta modulation of LG amplitude in the CA3 region during context exploration increases with learning. (*A*) Behavioral profile of a representative rat during learning of the task. Shown is the animal's performance (correct, black bar up; error, black bar down) at each trial of the session (*Upper*) and the associated learning curve computed by using a sliding window of 20 trials (*Lower*). (*B*) Pseudocolor scale representation of the mean CA3 LG amplitude as a function of the theta phase for each trial in the session (*Left*). The mean LG amplitude per theta phase averaged over the first and last 20 trials is also shown (*Right*). (*C*) MI curve computed by using a 20-trial sliding window. (*D*) Linear correlation study between theta-LG coupling strength and task performance. The correlation between the MI and learning curves (*Left*) and the average MI value over each mean performance percentage (*Right*) are shown. These results were derived from the average over electrodes located in the CA3 region of this representative animal (see Figs. S1 and S2 for group results).

Results

Theta-Phase Modulates the Low Gamma (LG) Subband in the CA3 Region. Local field potentials (LFPs) were recorded from tetrodes located in the CA3 pyramidal layer of the dorsal hippocampus of six freely moving rats. The existence of phase-amplitude CFCs was analyzed by using a comodulogram method as described (6). This tool scans several narrowed-filtered frequency bands pairs searching specifically for phase-amplitude coupling. The level of phase-amplitude coupling in each frequency pair is assessed by a measure called the modulation index (MI) (see *Materials and Methods*). Although computationally intensive, the scanning of several frequency pairs performed by the comodulogram analysis is ideal for searching for phase-amplitude couplings when no a priori assumptions are made about the "phase modulating" and the "amplitude-modulated" frequency bands.

The results are graphically illustrated in a pseudocolor plot representing the MI values obtained for the analyzed frequency pairs, wherein hot colors in a given coordinate (x, y) indicate that the phase of the x frequency modulates the amplitude of the y frequency. As shown in Fig. 1B, we observed substantial theta-phase modulation of the amplitude of oscillations in the gamma range during the context exploration phase of the task, confirming previous reports of theta-modulated gamma (6–9). In particular, this analysis revealed especially strong theta-phase modulation of the LG (30–60 Hz) subband in the CA3 region (Fig. 1B). Based on this preliminary result, we focused our systematic LFP analyses on wide-band-filtered theta and LG in CA3.

Theta–Gamma CFC in CA3 Increases During Learning and the Strength of CFC Correlates with Mean Performance Accuracy. Fig. 2A shows the gradual improvement in behavioral performance during learning for a single rat. An initial trial-by-trial quantification of theta–gamma comodulation revealed that the relationship between LG amplitude and theta phase increased over the course of the learning session (Fig. 2B). We also examined the relationship between theta–gamma modulation during context exploration and subsequent choice accuracy of the learning session by calculating the percentage correct and MI over sliding windows of 20 trials shifted

in steps of one trial (Fig. 2A and C). This analysis revealed that the intensity of theta–gamma coupling positively and significantly correlated with performance accuracy as the animal makes more correct responses during the course of learning (Fig. 2D). Theta–gamma coupling was also significantly higher during context exploration when mean performance accuracy was high ($\geq 80\%$) compared with coupling when performance accuracy was low ($\leq 60\%$) both within (Fig. S1a) and across animals [Fig. S1b; $F(1, 344) = 224.57, P < 10^{-20}$]. This result was robust across all learning sessions (Fig. S1d), wherein the mean correlation coefficient (r) between performance and MI was significantly different from zero [$r = 0.67 \pm 0.08$ (mean $\pm$ SEM), $t(5) = 8.66, P < 0.001$; see also Figs. S2 and S3). Because the MI scores for each window are not independent, we calculated the significance of the correlations against the distribution of r values calculated from 10,000 shuffles of trial and MI. We found that the observed r values could not have been derived from the chance distribution (Fig. S1c; $z = 3.5, P < 0.001$). Thus, when mean performance accuracy was high, theta was also more strongly coupled with LG during exploration of the context.

Increased Theta–Gamma Coupling Is Maintained During Overtraining Sessions. We next studied the level of theta–gamma coupling during sessions where the animals were overtrained on the conditional discrimination problem. In those sessions the rats' performance had been >80% for at least three consecutive preceding sessions on the same problem, such that very little new learning occurred during the recording session.

As shown in Fig. 3, the strength of theta–gamma CFC in overtraining sessions was high from the outset, and varied less during the overtraining session than during learning (Fig. 3 and Fig. S4). Moreover, whereas the average MI for the last 30 trials in learning sessions divided by the MI for the first 30 trials was 0.6, this MI ratio was close to 1 in overtraining sessions (Fig. 3B), indicating that the levels of theta–gamma coupling did not differ across the session in rats highly trained on the task [learning MI ratio: 0.596 ± 0.041 (mean $\pm$ SEM), $t(4) = -9.85, P < 0.001$ when compared with 1; overtraining MI ratio: 0.988 ± 0.039 (mean $\pm$ SEM), $t(4) =$
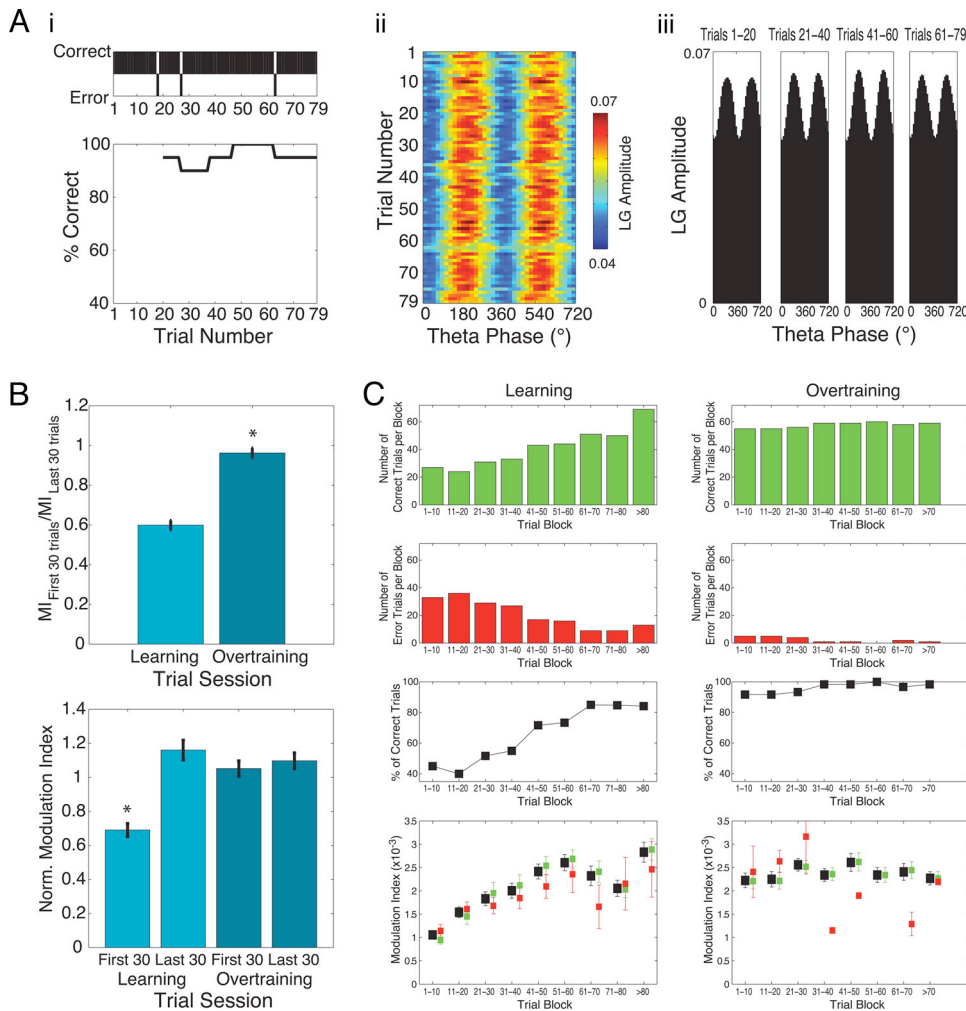
Fig. 3. Rats performing overtraining sessions maintain high levels of CA3 LG modulation by theta phase. (*A*) (*i*) Animal's performance during an overtraining session. (*ii*) Pseudocolor scale representation of the mean LG amplitude as a function of the theta phase for each trial in the overtraining session. (*iii*) Mean LG amplitude per theta phase in four nonoverlapping windows of 20 trials each. These results were obtained from a representative animal (see also Fig. S4). (*B*) Group data results. (*Upper*) MI ratio between the first and last 30 trials of learning and overtraining sessions. (*Lower*) Normalized MI for the first and last 30 trials of learning and overtraining sessions. The normalization was done within each group by dividing each group value by the average over the four groups. Bars represent the mean (± SEM) over rats. *, $P <$ 0.001. (*C*) Pooled data results. (*Upper Three Rows*) Shown are the number of correct (green) and error (red) trials pooled among all animals in nonoverlapping 10 trial blocks for learning (*Left*) and overtraining (*Right*) sessions, and the percentage of correct trials in each block. The mean MI value in each trial block is shown (black squares). (*Lower Row*) Also shown are the mean MI in each trial block separated for correct (green squares) and error (red squares) trials. Error bars represent SEM.

-0.32, $P = 0.76$ when compared with 1; difference between groups $t(4) = -8.54$, $P = 0.001$]. In addition, on average, the CFC levels observed during the last trials in learning sessions were comparable with the levels observed throughout overtraining sessions (Tukey posthoc, $P > 0.05$; Fig. 3*B*; see also Fig. 5*B*).

Of note, we observed that the MI values tended to increase for both correct and error trials during learning sessions (Fig. 3*C* and Fig. S5), and we found a positive correlation between trial number and MI value for errors ($r = 0.31$) or correct trials ($r = 0.32$; all trials $r = 0.35$, all $Ps < 0.0001$). During overtraining sessions, however, there were no statistical correlations between trial number and MI value for both error and correct trials (all $Ps > 0.18$). In all, these results suggest that stronger theta–gamma coupling persists as long as overall task performance is high.
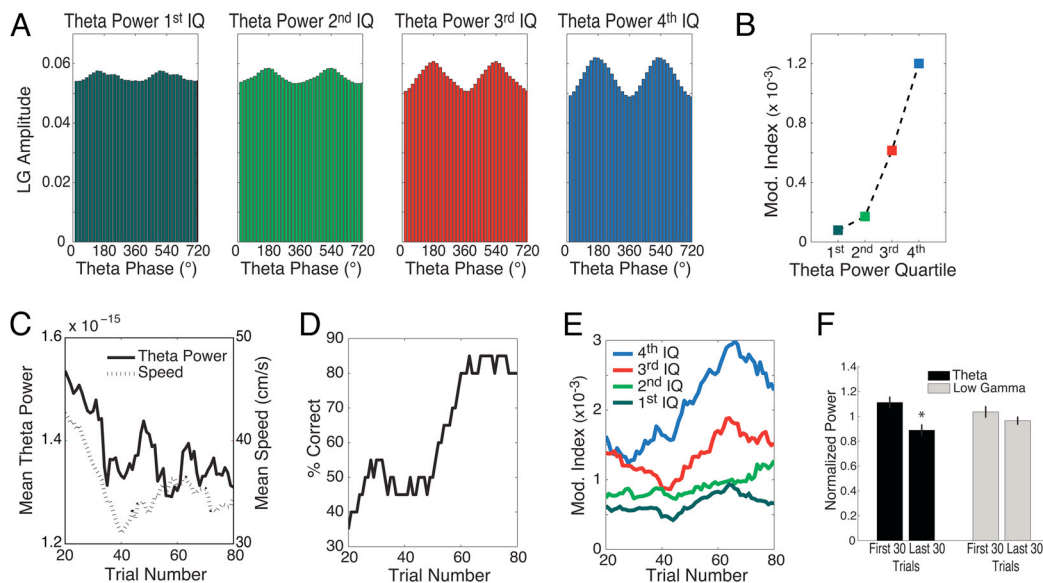
The Increase in Theta–Gamma Coupling Associated with Learning Cannot Be Explained by Changes in Theta Power, Speed of Locomotion, or Gamma Power. We next examined whether changes in theta power could account for the increase in theta–gamma phase-amplitude coupling during learning. It was previously shown that the intensity of the theta–gamma coupling depends on the magnitude of theta power such that theta–gamma coupling is stronger when theta power is high if other confounding variables are controlled (5, 6). We have confirmed this finding during context exploration in our current data, as shown in the example in Fig. 4 *A* and *B*. When LFP epochs were divided into four periods varying from lowest to highest theta power (see *Materials and Methods*) theta–gamma modulation strength monotonically increased with

theta power. Therefore, theta power level does influence the level of coupling and changes in theta power along the learning session could potentially account for the changes in theta–gamma coupling (but see below).

We also asked whether changes in running speed or path length across trials during the exploratory period could account for the increase in theta–gamma coupling. As expected, both running speed and path length significantly decrease across trial blocks in learning and overtraining sessions [path length: $F(2, 20) = 36.719$, $P < 0.00001$; speed: $F(2, 20) = 29.793$, $P < 0.00001$; see Fig. S6]. However, the change of the speed and path length did not differ significantly between learning and overtrained sessions [interaction of trial block with session type; path length: $F(2, 20) = 2.034$, $P = 0.157$; speed: $F(2, 20) = 1.217$, $P = 0.296$]. Therefore, the observation that rats slow and move less during the course of performing in both learning and overtraining sessions does not account for the selective increase in theta–gamma coupling only in learning sessions.

There are also reports that the hippocampal theta power and a rat's running speed can be positively correlated (19, 20). Therefore, the observed increase in theta–gamma coupling during learning could be caused by an increase in either theta power or locomotion speed during late trials in the session. However, our observations were opposite to this prediction: both theta power and speed decrease (Fig. 4*C*) as the animal's performance accuracy increases (Fig. 4*D*). Moreover, the levels of theta–gamma phase-amplitude coupling increased during the learning session when the MI analysis was restricted (within each trial) to any of the four theta power-level

Fig. 4. Theta-phase modulation of LG amplitude is positively related to theta power, but changes in theta power level across trials do not account for the increase in theta–gamma coupling with learning. (*A*) Mean LG amplitude per theta phase for periods of low [first interquartile (IQ) interval], medium (second and third IQ), and high (fourth IQ) theta power, which were defined within each trial. These results were obtained from a representative CA3 electrode by analyzing all trials (*n* = 80) in a learning session. (*B*) MI computed for each case shown in *A*. (*C*) Theta power in this electrode as a function of the trial number. A sliding window of 20 trials was used, and each point is the average theta power over the 20 trials. The mean rat's speed is also shown (dashed line, right *y*-scale). (*D*) Learning curve of this animal. (*E*) MI curves computed for each theta power quartile. (*F*) Group results showing the theta and LG CA3 power levels during the first and last 30 trials of learning sessions. The power normalization was done within rats by dividing each power value by the average power over the two groups of trials. Bars represent the mean (± SEM) over rats. *, $P < 0.05$.

periods (Fig. 4*E*). Of note, gamma power did not vary during learning (Fig. 4*F*), so it is also unlikely to account for the observed changes in the strength of theta–gamma phase-amplitude CFC with learning. Taken together, these findings indicate that the increase in theta–gamma coupling cannot be explained by changes in theta power, running speed, or gamma power.

The Learning-Related Changes in the Level of Theta–Gamma Coupling Persist Until Stimulus Sampling and Selection. The above analyses have been focused on the context exploratory period of the task (see Fig. 1*A*), when the rat must recognize which context it occupies to subsequently choose the correct stimulus. We also analyzed CFC on the LFPs recorded during the choice period of the task, when the
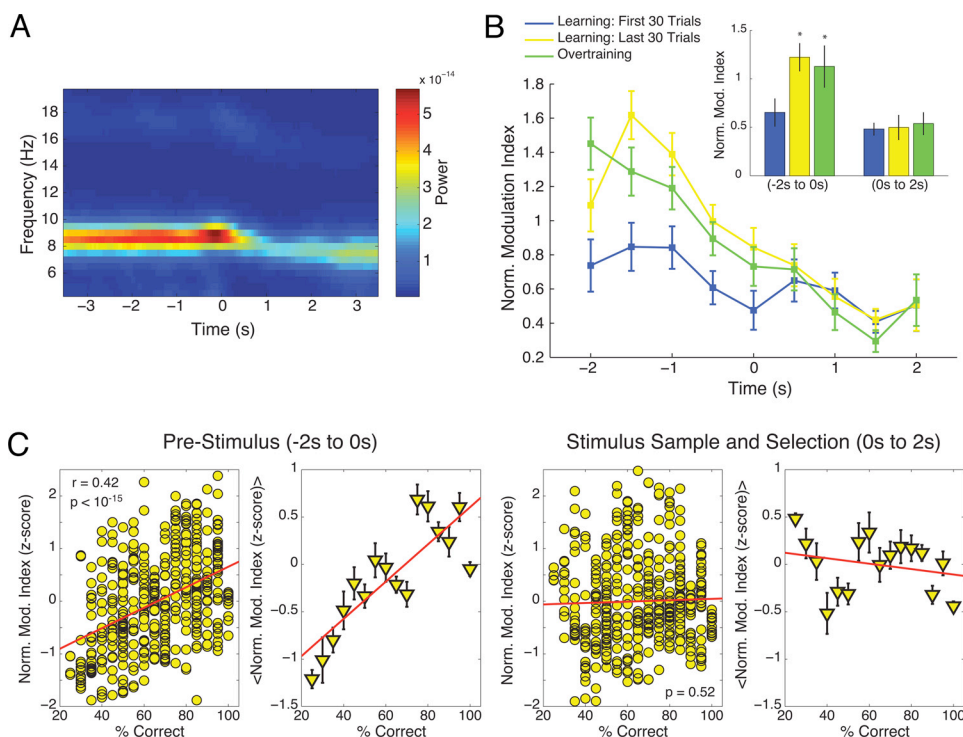
Fig. 5. The strength of theta–gamma coupling correlates with learning up to stimulus sampling. (*A*) Time-frequency decomposition of a representative fissure electrode during the choice period of the task. The time point 0 denotes the initiation of stimulus sampling, defined as the crossing of the rat's nose over the rim of the pot (see *Materials and Methods*). (*B*) Normalized MI during the choice period of the task. The normalization was done within each rat by dividing the MI value of each group by the average MI over groups. Data points represent the mean (± SEM) over rats. *, $P < 0.05$. (*C*) Linear correlation of the pooled data around the period of stimulus sampling and selection.

rat is presented with the two stimuli and must select the stimulus associated with that context to obtain a reward.

The results of these analyses are shown in Fig. 5. Theta power was high as the rats walked toward the scented pot. However, theta power and peak theta frequency were reduced when the rats stopped to sample (i.e., sniff) the stimulus and dig for reward (Fig. 5*A*). Theta–gamma phase-amplitude coupling was also greatly reduced during digging (Fig. 5*B*). Moreover, while the learning-related changes in the level of theta–gamma CFC observed during context exploration were present while rats were approaching the item (Fig. 5 *B* and *C*), the strength of theta–gamma coupling during stimulus sampling and selection did not change during learning (Fig. 5*B*) nor was the strength of CFC correlated with performance (Fig. 5*C*). These results therefore suggest that theta–gamma coupling could be promoting memory recall up to when the animals sample the stimulus items.

Discussion

Our results strongly suggest a functional role for the theta-phase modulation of the gamma amplitude in the CA3 region. The strength of theta–gamma coupling increased during learning (Fig. 2 and Fig. S1) and remained high in overtraining sessions (Fig. 3 and Fig. S4 and S5). Correspondingly, the magnitude of theta–gamma CFC during context exploration was correlated with the high accuracy of behavioral performance, which increased during the course of learning (Fig. 2 and Figs. S1–S3). These findings support the view that the theta–gamma interaction contributes to memory processing (10, 14, 21).

The present results also constitute neurophysiological evidence corroborating a role of the rodent hippocampus in learning about what happens where (17, 18) and points to CA3 as an important region for this type of associative memory. These findings are consistent with previous proposals suggesting that the CA3 region combines converging information about events and the context in which they occur (22), which is required for the learning of new associations in the present task.

Phase-amplitude coupling of neuronal oscillations has been gaining interest during the last few years (4–6, 23–25). Phase-amplitude CFCs have been described in mice (8, 9, 26), rats (7), monkeys (4), and humans (5, 24, 25) and in multiple brain regions including neocortex (4, 5, 25), hippocampus (7), and basal ganglia (6, 24). Phase-amplitude CFCs have also recently been described across different brain regions (6, 23), suggesting that they may be also involved in long-range information processing. Although the exact functional significance of CFC remains unclear, some have suggested that the coupling of low- and high-frequency brain oscillations subserves sensory signal detection (27) and attention selection (28). Surprisingly, no compelling evidence has been previously shown for a functional role for the best-known example of CFC, namely the theta–gamma coupling observed in the rodent hippocampus, despite a wealth of theoretical work attempting to link this phenomenon to hippocampal function in learning and memory (10–15, 21). The present work constitutes empirical evidence that the theta–gamma CFC in the hippocampus supports cognitive functions, specifically memory processing, as suggested by the models (10–15, 21).

Although our findings are consistent with the proposal that theta–gamma interaction functions as a memory code (10, 14, 21), our findings do not shed light on how the higher modulation of the gamma amplitude by the theta phase supports memory. The knowledge about the biophysical mechanisms underlying such effects might provide important clues (26, 29). Nevertheless, the data provide some potential insights into cognitive processing during performance on the task. Notably, levels of theta–gamma phase-amplitude coupling increased during learning for both error and correct trials (Fig. 3*C* and Fig. S5). A possible explanation for this observation is that error trials may reflect a miscoding of information, which would be reflected in strong CFC and lead

actively to an incorrect response (30), rather than the absence of coding, wherein one might expect weak CFC and guessing. The higher levels of coupling seen for error trials after learning and during overtrained sessions also suggest that theta–gamma coupling in the hippocampus is unlikely to play a role in attentional modulation (but see ref. 28).

It still remains to be established whether theta–gamma coupling would be more functionally important than either of these two rhythms alone. We found that the level of gamma power was not correlated with performance accuracy [$r = 0.08 \pm 0.31$ (mean $\pm$ SEM)], whereas the decrease in theta power along the learning session presented a negative correlation [$r = -0.54 \pm 0.19$ (mean $\pm$ SEM)]. Although the decrease in theta power is likely associated with the decrease in locomotion along the session, a functional role for the levels of theta power in this task cannot be ruled out.

The association of specific events with the context in which they occur is known to be a function of the rodent hippocampus (31, 32), although the mechanisms by which these associations are generated in the hippocampus are only beginning to become clear (17). Studies using the same conditional discrimination paradigm have revealed that the hippocampus is critical for this kind of learning (18) and that hippocampal principal cells encode conjunctive representations of items and places in a way that parallels learning and predicts performance accuracy (17). Here, we extend these findings by showing a direct correlation between theta–gamma CFC strength, learning, and the consequent increase in performance accuracy. Furthermore, the present results are consistent with the notion that the theta–gamma interaction subserves a role in information coding of relevance to successful recall required for accurate performance.

Materials and Methods

Training and Data Acquisition. Behavioral training and electrophysiology recording methods are described in detail in ref. 17 and reproduced in *SI Text*. During all recording sessions, LFPs were obtained from tetrodes located in the pyramidal cell layer of CA3 (see *SI Text* and Fig. S7); the signals were filtered from 1 to 300 Hz and sampled at a rate of 1,000 samples per s. Behavior was recorded with digital video (30 frames per s) that was synchronized with the acquisition of neural data. The onset of stimulus sampling (time 0 in Fig. 5) was defined as the video frame on which the rat's nose crossed the rim of the pot. The LFPs and the time stamps for the onset of stimulus sampling were imported into MATLAB (Mathworks) for subsequent data analysis.

Data Analysis. All analyses were done with built-in and custom-written routines in MATLAB.

Spectral Analyses, Filter Settings, and Amplitude and Phase Time Series Extraction. Power spectra estimation during the exploratory period of the task was done by means of the Welch periodogram method (50% overlapping Hamming windows with a length of 2 s), which was obtained by using the *pwelch* function from the Signal Processing Toolbox. The time frequency decomposition during the choice period of the task shown in Fig. 5*A* used 1-s time windows with 95% overlap and was obtained by using the *spectrogram* function from the Signal Processing Toolbox. All filtering used for the data analysis was done by means of a linear finite impulse response filter using the *eegfilt* routine from the EEGLAB toolbox (33). The filter order depends on the low-frequency cutoff, and it is given by three times the ratio of the sampling frequency to the low-frequency cutoff (rounded to the nearest integer toward zero). Both the instantaneous amplitude and the phase time series of a filtered signal were computed from the Hilbert transform, which was obtained by using the *hilbert* routine from the Signal Processing Toolbox. The amplitude envelope of the theta-filtered signal (i.e., the instantaneous theta power) was used in Fig. 4 for dividing the time series of each trial into four quartiles. The instantaneous theta power was also used to determine the mean theta power in each trial, and the reported results during the context exploration were obtained from analyzing the trial periods where theta power was above its mean value (except in Fig. 4). However, the same qualitative results were obtained when no prior selection of "high-theta" periods was performed (see Fig. S8).

The MI and the Phase-Amplitude Comodulogram. To measure the intensity of theta-LG phase-amplitude coupling, we used a MI as described (6). This index is

calculated as follows: (*i*) the theta phases are binned into 18 20° intervals (0–360°) and the mean amplitude of the LG oscillation in each phase bin is determined; (*ii*) this result is then normalized by dividing the mean amplitude in each phase bin by the sum over the bins. This last step thus transforms the mean amplitude per phase into a probability distribution-like function (see Figs. 2*B*, 3*A*, and 4*A* for examples); (*iii*) then the Kullback-Leibler (KL) distance (34), a measure that is widely used to infer the distance between two distributions, was used to measure how much the phase-amplitude distribution deviates from the uniform distribution. The MI is obtained by dividing the KL distance by a constant factor [log(18), i.e., the logarithm of the number of phase bins], which makes the measure assume values between 0 and 1. Therefore, a MI value of 0 denotes that the phase-amplitude distribution is equal to the uniform distribution; that is, in this case the mean amplitude is the same for all phase bins, which characterizes the absence of phase-amplitude coupling. The further away the amplitude distribution gets from the uniform distribution (as inferred by the KL distance), the higher the MI. The comodulgram plot shown in Fig. 1*B* was obtained by applying the MI measure to several narrowed-filtered frequency pairs (phase frequencies: 4-Hz bandwidths and 2-Hz steps; amplitude frequencies: 10-Hz bandwidths and 5-Hz steps) and expressing the results by a pseudocolor code scheme (see also ref. 6). For the other figures, the MI was calculated between the 6- to 10-Hz (theta) and 30- to 55-Hz (LG) frequency bands.

Learning and MI Curves. The learning curve was computed by calculating the percentage of correct choices in sliding trial windows of 20 trials shifted in steps of one trial. The MI curve is obtained by computing the mean MI over all 20 trials in each trial window used to compute the learning curve. The MI curve of each rat is computed from mean MI curve over all eligible electrodes in that rat; in practice, all CA3 electrodes tend to present similar MI curves (see Fig. S8).

MI Computation During Item Sampling. Given the brief duration of the stimulus sampling periods, the MI during the choice period of the task shown in Fig. 5 was computed by using phase and amplitude time series merged across all trials (as in ref. 6). In Fig. 5*B*, each MI time point denotes the MI value for a time window of 1 s ending on the time point (therefore, for each rat, the MI time points during the first 30-trial block were obtained from the analysis of a 30-s time series). The MI values shown in Fig. 5 *B Inset* and *C* were computed by using the time interval as denoted in the figure's labels.

Statistical and Correlation Analyses. Comparisons of the MI between groups were done by using a *t* test or ANOVA followed by Tukey's test, as appropriate. Linear correlations were measured by using the Pearson correlation coefficient. $P < 0.05$ level of confidence was used in these analyses.

1. Buzsaki G, Draguhn A (2004) Neuronal oscillations in cortical networks. *Science* 304:1926–1929.
2. Buzsaki G (2006) *Rhythms of the Brain* (Oxford Univ Press, New York).
3. Jensen O, Colgin LL (2007) Cross-frequency coupling between neuronal oscillations. *Trends Cognit Sci* 11:267–269.
4. Lakatos P, et al. (2005) An oscillatory hierarchy controlling neuronal excitability and stimulus processing in the auditory cortex. *J Neurophysiol* 94:1904–1911.
5. Canolty RT, et al. (2006) High gamma power is phase-locked to theta oscillations in human neocortex. *Science* 313:1626–1628.
6. Tort AB, et al. (2008) Dynamic cross-frequency couplings of local field potential oscillations in rat striatum and hippocampus during performance of a T-maze task. *Proc Natl Acad Sci USA* 105:20517–20522.
7. Bragin A, et al. (1995) Gamma (40–100 Hz) oscillation in the hippocampus of the behaving rat. *J Neurosci* 15:47–60.
8. Buzsaki G, et al. (2003) Hippocampal network patterns of activity in the mouse. *Neuroscience* 116:201–211.
9. Hentschke H, Perkins MG, Pearce RA, Banks MI (2007) Muscarinic blockade weakens interaction of gamma with theta rhythms in mouse hippocampus. *Eur J Neurosci* 26:1642–1656.
10. Jensen O, Idiart MA, Lisman JE (1996) Physiologically realistic formation of autoassociative memory in networks with theta/gamma oscillations: Role of fast NMDA channels. *Learn Mem* 3:243–256.
11. Jensen O, Lisman JE (1996) Theta/gamma networks with slow NMDA channels learn sequences and encode episodic memory: Role of NMDA channels in recall. *Learn Mem* 3:264–278.
12. Lisman J (2005) The theta/gamma discrete phase code occuring during the hippocampal phase precession may be a more general brain coding scheme. *Hippocampus* 15:913–922.
13. Lisman J, Buzsaki G (2008) A neural coding scheme formed by the combined function of gamma and theta oscillations. *Schizophr Bull* 34:974–980.
14. Lisman JE, Idiart MA (1995) Storage of 7 +/− 2 short-term memories in oscillatory subcycles. *Science* 267:1512–1515.
15. Lisman JE, Talamini LM, Raffone A (2005) Recall of memory sequences by interaction of the dentate and CA3: A revised model of the phase precession. *Neural Netw* 18:1191–1201.
16. Senior TJ, Huxter JR, Allen K, O'Neill J, Csicsvari J (2008) Gamma oscillatory firing reveals distinct populations of pyramidal cells in the CA1 region of the hippocampus. *J Neurosci* 28:2274–2286.
17. Komorowski R, Manns J, Eichenbaum H (2009) Robust conjunctive item-place coding by hippocampal neurons parallels learning what happens where. *J Neurosci* 29:9918–9929.
18. Rajji T, Chapman D, Eichenbaum H, Greene R (2006) The role of CA3 hippocampal NMDA receptors in paired associate learning. *J Neurosci* 26:908–915.
19. DeCoteau WE, et al. (2007) Learning-related coordination of striatal and hippocampal theta rhythms during acquisition of a procedural maze task. *Proc Natl Acad Sci USA* 104:5644–5649.
20. Montgomery SM, Betancur MI, Buzsaki G (2009) Behavior-dependent coordination of multiple theta dipoles in the hippocampus. *J Neurosci* 29:1381–1394.
21. Jensen O, Lisman JE (1996) Novel lists of 7 +/− 2 known items can be reliably stored in an oscillatory short-term memory network: Interaction with long-term memory. *Learn Mem* 3:257–263.
22. Lisman JE (1999) Relating hippocampal circuitry to function: Recall of memory sequences by reciprocal dentate–CA3 interactions. *Neuron* 22:233–242.
23. Sirota A, et al. (2008) Entrainment of neocortical neurons and gamma oscillations by the hippocampal theta rhythm. *Neuron* 60:683–697.
24. Cohen MX, et al. (2009) Good vibrations: Cross-frequency coupling in the human nucleus accumbens during reward processing. *J Cognit Neurosci* 21:875–879.
25. Cohen MX, Elger CE, Fell J (2009) Oscillatory activity and phase-amplitude coupling in the human medial frontal cortex during decision making. *J Cognit Neurosci* 21:390–402.
26. Wulff P, et al. (2009) Hippocampal theta rhythm and its coupling with gamma oscillations require fast inhibition onto parvalbumin-positive interneurons. *Proc Natl Acad Sci USA* 106:3561–3566.
27. Handel B, Haarmeier T (2009) Cross-frequency coupling of brain oscillations indicates the success in visual motion discrimination. *NeuroImage* 45:1040–1046.
28. Schroeder CE, Lakatos P (2009) Low-frequency neuronal oscillations as instruments of sensory selection. *Trends Neurosci* 32:9–18.
29. Tort AB, Rotstein HG, Dugladze T, Gloveli T, Kopell NJ (2007) On the formation of gamma-coherent cell assemblies by oriens lacunosum-moleculare interneurons in the hippocampus. *Proc Natl Acad Sci USA* 104:13490–13495.
30. Deadwyler SA, Bunn T, Hampson RE (1996) Hippocampal ensemble activity during spatial delayed-nonmatch-to-sample performance in rats. *J Neurosci* 16:354–372.
31. Eichenbaum H, Dudchenko P, Wood E, Shapiro M, Tanila H (1999) The hippocampus, memory, and place cells: Is it spatial memory or a memory space? *Neuron* 23:209–226.
32. Eichenbaum H, Yonelinas AP, Ranganath C (2007) The medial temporal lobe and recognition memory. *Annu Rev Neurosci* 30:123–152.
33. Delorme A, Makeig S (2004) EEGLAB: An open source toolbox for analysis of single-trial EEG dynamics including independent component analysis. *J Neurosci Methods* 134:9–21.
34. Santner T, Duffy D (1989) *The Statistical Analysis of Discrete Data* (Springer, New York).

NEUROSCIENCE